Noncatalytic Assembly of Ribonuclease III with Double-Stranded RNA

Jaroslaw Blaszczyk, Jianhua Gan,
Joseph E. Tropea, Donald L. Court,
David S. Waugh, and Xinhua Ji*
Center for Cancer Research
National Cancer Institute
National Institutes of Health
Frederick, Maryland 21702

Summary

**Ribonuclease III (RNase III) represents a family of dou-
ble-stranded RNA (dsRNA) endonucleases. The simplest
bacterial enzyme contains an endonuclease domain
(endoND) and a dsRNA binding domain (dsRBD).
RNase III can affect RNA structure and gene expres-
sion in either of two ways: as a dsRNA-processing
enzyme that cleaves dsRNA, or as a dsRNA binding
protein that binds but does not cleave dsRNA. We pre-
viously determined the endoND structure of *Aquifex aeo-
licus* RNase III (Aa-RNase III) and modeled a catalytic
complex of full-length Aa-RNase III with dsRNA. Here,
we present the crystal structure of Aa-RNase III in
complex with dsRNA, revealing a noncatalytic assem-
bly. The major differences between the two functional
forms of RNase III·dsRNA are the conformation of the
protein and the orientation and location of dsRNA. The
flexibility of a 7 residue linker between the endoND
and dsRBD enables the transition between these two
forms.**

Introduction

Double-stranded RNA (dsRNA) influences critical cell
functions. Ribonuclease III (RNase III) belongs to the
family of dsRNA-specific endoribonucleases (Court, 1993;
Robertson et al., 1968) and has been found in all studied
prokaryotes and eukaryotes (Court, 1993; Filippov et al.,
2000; Krainer, 1997; Nicholson, 1996, 1999). RNase IIIs
range in length between ∼200 and ∼2000 amino acid
residues (Figure 1A) and play important roles in RNA
processing, posttranscriptional gene expression control
(Court, 1993; Krainer, 1997; Wu et al., 2000), cellular
defense against viral infection (Court, 1993; Robertson
et al., 1968), and RNA interference (RNAi) (Bernstein et
al., 2001; Carthew, 2001). *Escherichia coli* RNase III (Ec-
RNase III) is the simplest member of the family, con-
sisting of an endonuclease domain (endoND) followed
by a dsRNA binding domain (dsRBD). RNase III from
Saccharomyces cerevisiae (Sc-Rnt1p) is composed of
an endoND, a dsRBD, and an additional N-terminal do-
main of ∼200 amino acid residues with no known func-
tion (Lamontagne et al., 2001). *Drosophila melanogaster*
RNase III (Dm-Drosha) has two endoNDs, one dsRBD,
and a larger N-terminal extension of ∼900 amino acid

residues (Filippov et al., 2000). *Homo sapiens* RNase III
(Hs-Dicer) consists of two endoNDs, one dsRBD, and
an even larger N-terminal extension of ∼1500 amino acid
residues, which includes a PAZ domain and a helicase
domain (Bernstein et al., 2001) (Figure 1A). The sequence
of the endoND is characterized by nine highly conserved
amino acid residues known as the RNase III signature
motif (Figure 1B).

RNase III influences gene expression from mRNA as
either a dsRNA-processing enzyme or a dsRNA binding
protein (Dasgupta et al., 1998; Oppenheim et al., 1993).
As a dsRNA-processing enzyme, RNase III degrades
both natural and synthetic dsRNA to small duplex prod-
ucts averaging 10–18 base pairs (bp) in length (Court,
1993; Dunn, 1982; Robertson, 1982; Robertson and Dunn,
1975). As a dsRNA binding protein, Ec-RNase III binds
certain substrates without processing and still influ-
ences gene expression (Dasgupta et al., 1998; Oppen-
heim et al., 1993). RNase III has received a significant
amount of attention as a dsRNA-processing enzyme but
not much as a dsRNA binding protein. Two forms of the
RNase III·dsRNA complex may exist. One takes the form
of a catalytic complex in which the bound dsRNA is
contacting the endoND active center (Blaszczyk et al.,
2001). The other takes the form of a noncatalytic assem-
bly in which the endoND active center may not be asso-
ciated with the bound dsRNA. Ten missense mutations
that cause defects in Ec-RNase III have been identified
and their effects elucidated (Figure 1B), among which
rnc70 (E117K, corresponding to E110K in Aa-RNase III)
creates a mutant RNase III protein with impaired endo-
nucleolytic activity but without blocking its ability to
recognize and bind dsRNA in vivo or in vitro (Court,
1993; Dasgupta et al., 1998; Inada et al., 1989; Li and
Nicholson, 1996). Therefore, this mutant may form a
noncatalytic assembly with dsRNA.

Structural information that relates to RNase III has
been accumulating since 1995. In addition to the NMR
solution structures of dsRBDs in Ec-RNase III and other
dsRNA binding proteins (Bycroft et al., 1995; Kharrat et
al., 1995; Nanduri et al., 1998; Ramos et al., 2000), a
crystal structure was determined for a dsRBD of *Xeno-
pus laevis* RNA binding protein A in complex with dsRNA
(Xl-dsRBD·dsRNA) (Ryter and Schultz, 1998). We pre-
viously reported the endoND structure of *Aquifex aeoli-
cus* RNase III in its ligand-free form (Aa-endoND) and
in complex with Mn^{2+} (Aa-endoND·Mn^{2+}), providing the
first glimpse at the RNase III active site (Blaszczyk et
al., 2001; Zamore, 2001). Recently, the crystal structure
of a hypothetical RNase III (Tm1102) from *Thermotoga
maritima* (Tm-RNase III) was determined by the Joint
Center for Structural Genomics (PDB entry 1O0W, Figure
1B). Here, we present two crystal structures: that of the
wild-type endoND of Aa-RNase III in complex with Mg^{2+}
(Aa-endoND·Mg^{2+}) and that of full-length Aa-RNase III
(E110K) with bound dsRNA (Aa-E110K·dsRNA). The se-
quence of the dsRNA we cocrystallized with Aa-E110K
is the same as that used in Xl-dsRBD·dsRNA (Ryter
and Schultz, 1998), which allows a direct comparison of

*Correspondence: jix@ncifcrf.gov

A

Hs-Dicer

Dm-Drosha

Sc-Rnt1p

Ec-RNase III

B

```
                    α1                 α2              α2′
Aa-RNase III  .....MKMLE QLEKKLGYTF KDKSLLEKAL THVSYS.... ...KK..EHY   36
Tm-RNase III  MNESERKIVE EFQKETGINF KNEELLFRAL CHSSYANEQN QAGRKDVESN   50
Ec-RNase III  MN...PIVIN RLQRKLGYTF NHQELLQQAL THRSAS.... ...SK...HN   37

                    α3                  α4              α5
Aa-RNase III  ETLEFLGDAL VNFFIVDLLV QYSPNKREGF LSPLKAYLIS EEFFNLLAQK   86
Tm-RNase III  EKLEFLGDAV LELFVCEILY KKYPEAEVGD LARVKSAAAS EEVLAMVSRK  100
Ec-RNase III  ERLEFLGDSI LSYVIANALY HRFPRVDEGD MSRMRATLVR GNTLAELARE   87
                       1  2

              3₁₀       α5′     3₁₀                α6              α7
Aa-RNase III  LELHKFIRIK RG..KIN... .ETIIGDVFE ALWAAVYIDS GRDANFTREL  130
Tm-RNase III  MNLGKFLFLG KGEEKTGGRD RDSILADAFE ALLAAIYLDQ GYEK..IKEL  148
Ec-RNase III  FELGECLRLG PGELKSGGFR RESILADTVE ALIGGVFLDS DIQT..VEKL  135
                     3                               4

              α7                        α8              β1     3₁₀
Aa-RNase III  FYKLFKEDIL SAIKEGRVKK DYKTILQEIT QKRWKERPEY RLISVEGPHH  180
Tm-RNase III  FEQEF.EFYI EKIMKGEMLF DYKTALQEIV QSEHKVPPEY ILVRTEKNDG  197
Ec-RNase III  ILNWY.QTRL DEISPGDKQK DPKTRLQEYL QGRHLPLPTY LVVQVRGEAH  184
                                       5  6

               β2           β3                α9
Aa-RNase III  KKKFIVEAKI K..EYRTLGE GKSKKEAEQR AA.EELIKLL EESE        221
Tm-RNase III  DRIFVVEVRV NG..KTIATGK GRTKKEAEKE AARIAYEKLL KERS        240
Ec-RNase III  DQEFTIHCQV SGLSEPVVGT GSSRRKAEQA AAEQALKKLE LE..         226
                                             7
```

Figure 1. RNase III Proteins and Sequences

(A) Representatives of RNase III proteins: Hs-Dicer (1924 amino acid residues, GenBank AB028449), Dm-Drosha (1327 amino acid residues, SWISS-PROT Q9XYN5), Sc-Rnt1p (471 amino acid residues, SWISS-PROT Q02555), and Ec-RNase III (226 amino acid residues, SWISS-PROT P05797). The scale on top indicates the lengths of polypeptide chains. Cyan box represents helicase domain, green box PAZ domain, red box endoND, and blue box dsRBD. Additional domain structures in Hs-Dicer and Dm-Drosha are not shown.

(B) Sequence alignment of Aa-RNase III (SWISS-PROT O67082), Tm-RNase III (SWISS-PROT Q9X0I6), and Ec-RNase III (SWISS-PROT P05797). Secondary structural elements are indicated with shading, helices in green and strands in blue. Boxed amino acid residues at the C termini are not observed. Underlined is the RNase III signature motif. Shaded in red are seven Ec-RNase III residues for which data is available for ten mutant proteins, including (1) G44D (*rnc105* [Bardwell et al., 1989; Nashimoto and Uchida, 1985]); (2) I47N (*rnc⁻*; H.K. Peters, N. Costantino, and D.L.C., unpublished data]); (3) G97E (*rnc97* [Davidov et al., 1993]); (4) E117K (*rnc70* [Dasgupta et al., 1998; Inada et al., 1989; Li and Nicholson, 1996]), E117A (Li and Nicholson, 1996), and E117Q and E117D (Sun and Nicholson, 2001); (5) Q153P (*rnc10* [Inada and Nakamura, 1995]); (6) D155E (*rnc7* [Inada and Nakamura, 1995]); and (7) A211V (*rev3* [Nashimoto and Uchida, 1985]).

dsRBD-dsRNA interactions between these two protein types.

Results and Discussion

The Mg²⁺ and Mn²⁺ Ions Occupy the Same Binding Site with Identical Coordination

A divalent metal ion (preferably Mg^{2+}) is required for the reaction catalyzed by RNase III (Dunn, 1982; Li and Nicholson, 1996; Robertson et al., 1968; Sun and Nicholson, 2001). A comparison between the crystal structure of Aa-endoND·Mn^{2+} (Blaszczyk et al., 2001) and that of Aa-endoND·Mg^{2+} (this work) demonstrates that Mg^{2+} and Mn^{2+} occupy the same metal binding site with identical coordination that involves E40, D44, D107, and E110.

The E110K Mutation Influences the Binding of Both Mg²⁺ and dsRNA

As we previously proposed, six negatively charged side chains (E37, E40, D44, E64, D107, and E110) are clustered at each end of the catalytic valley upon dimerization of the endoND, forming two compound active centers (Blaszczyk et al., 2001). The same general structure of the endoND is found in the Aa-E110K·dsRNA complex. The electron density within one active center for
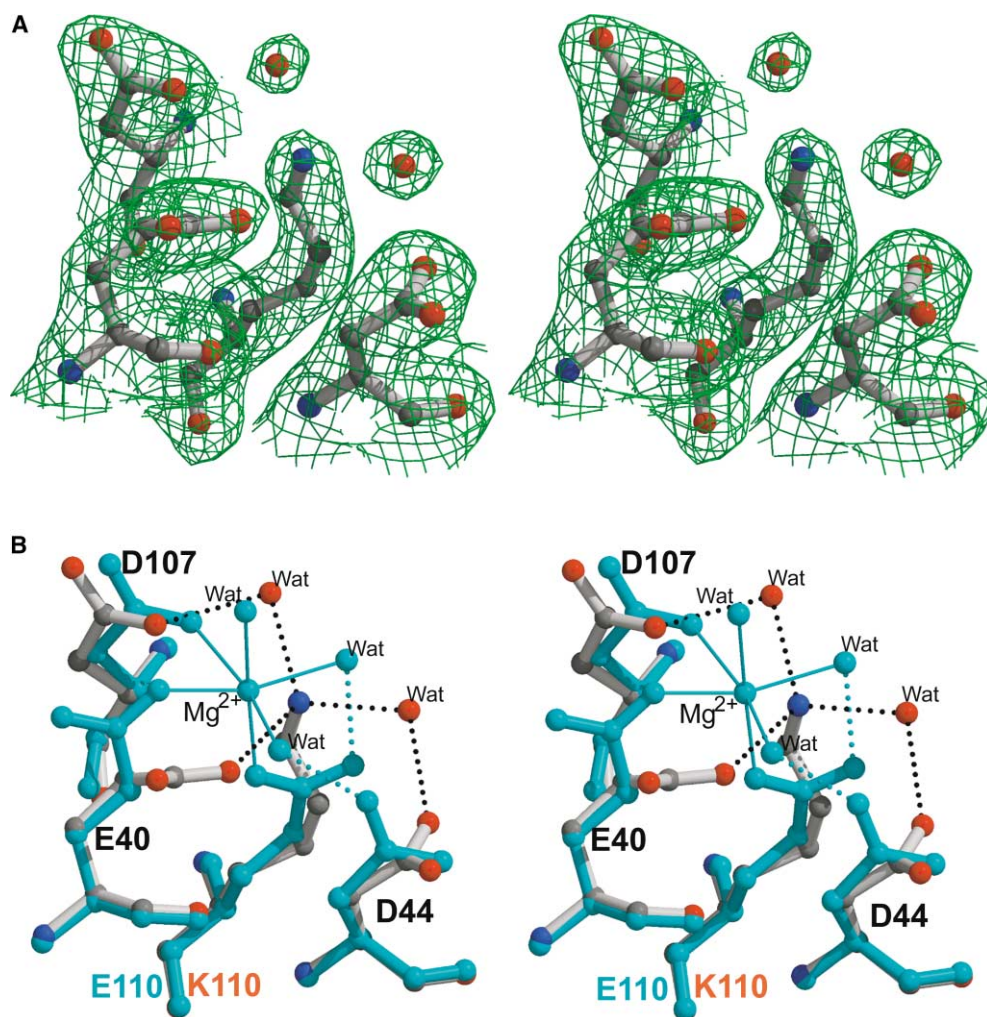
Figure 2. Impact of E110K Mutation on the Mg^{2+} Binding Site of Aa-RNase III

(A) Stereoview of the final 2F$_o$-F$_c$ electron density contoured at 1σ (green net) for the Aa-E110K mutation site. Residues E40, D44, D107, and K110, and two water molecules are illustrated as ball-and-stick models in atomic colors (gray carbon, blue nitrogen, and red oxygen).
(B) Stereoview showing the superposition of Aa-endoND·Mg^{2+} (in cyan) and Aa-E110K·dsRNA (in atomic colors). The coordination bonds of Mg^{2+} are shown as solid lines and hydrogen bonds as dashed lines.

the mutation site in the Aa-E110K·dsRNA structure is shown in Figure 2A. Although the Aa-E110K·dsRNA crystal was grown in the presence of 1.5 mM Mg^{2+} (Experimental Procedures), no Mg^{2+} was observed in the Aa-E110K·dsRNA structure. The mutation has two direct effects on the local environment relative to wild-type Aa-RNase III. First, it eliminates one negative charge from each active center. Second, atom NZ of K110 essentially occludes the Mg^{2+} binding site and forms a hydrogen bond network involving E40, D44, D107, and two water molecules (Figure 2B), rendering this environment in Aa-E110K no longer suitable for the binding of Mg^{2+}. Without the required Mg^{2+} ion, the endoND catalytic centers of Aa-E110K (Ec-E117K) cannot be functional in terms of RNA cleavage. Since the divalent metal ion enhances dsRNA binding (Li and Nicholson, 1996; Sun and Nicholson, 2001), without bound Mg^{2+}, the remaining negative charges at the active center of

Aa-E110K appear unfavorable for the binding of dsRNA within the active center, thereby giving rise to a distinct dsRNA binding form.

The dsRNA in Aa-E110K·dsRNA Is Not Bound in the Catalytic Valley

As described previously (Ryter and Schultz, 1998), the self-complementary RNA 10-mer (GGCGCGCGCC) forms 10 bp dsRNA helices, which stack end-to-end as a pseudocontinuous helix in the crystal lattice. Each Aa-E110K monomer binds two consecutive 10 bp dsRNA helices in the pseudocontinuous helix, forming the content of the asymmetric unit. Because RNase III functions as a dimer, a dimer of the Aa-E110K·dsRNA complex is shown in Figure 3. The secondary structure assignment for the entire polypeptide chain is diagrammed in Figure 1B and labeled in part in Figure 3A. As previously established (Blaszczyk et al., 2001), seven α-helices and one
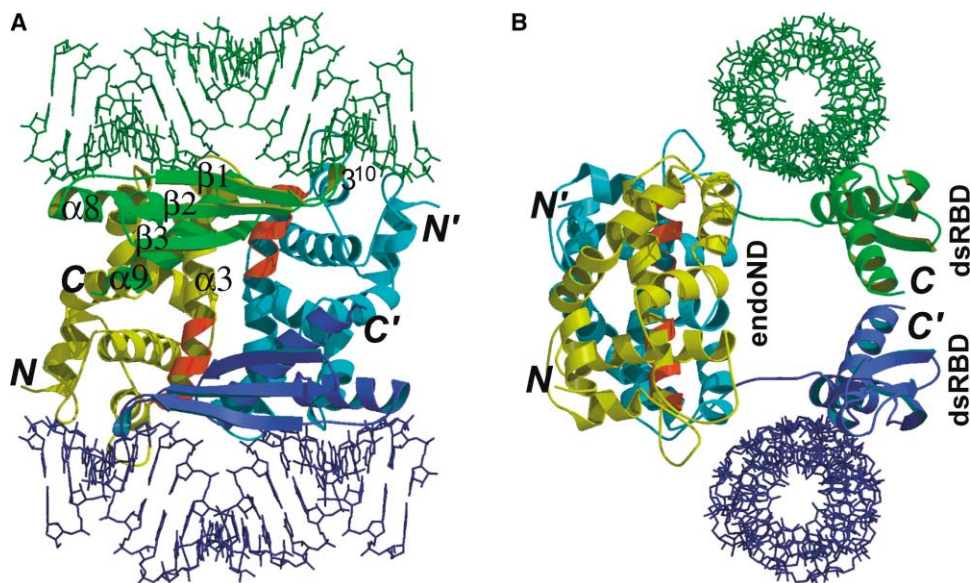
Figure 3. Overall Structure of Aa-E110K·dsRNA

(A) Illustration of a biological dimer of the Aa-E110K·dsRNA complex. The crystallographically independent molecule and its symmetry mate are indicated by N-C, and N′-C′, respectively. Secondary structural elements are labeled for those in dsRBD and α3 in the endoND. The endoND, dsRBD, dsRNA, endoND^{sym}, dsRBD^{sym}, and dsRNA^{sym} are colored yellow, green, green, cyan, blue, and blue, respectively. The RNase III signature motif at the N terminus of α3 is highlighted in red. Helices, β strands and loops are drawn as spirals, arrows, and pipes, respectively.
(B) A different view of dimeric Aa-E110K·dsRNA related to the view in (A) by a 90° rotation around the vertical axis.

3_{10} helix are the building blocks for the Aa-endoND. The endoND of Tm-RNase III (PDB entry 1O0W) contains two more α-helices and one more 3_{10} helix (Figure 1B), whereas the secondary structural composition of the dsRBD is conserved between the Aa- and Tm-dsRBD (Figure 1B).

The crystal structure of Aa-E110K·dsRNA has three features. First, each dsRBD binds a different dsRNA helix. Second, neither of the two dsRNA helices associated with the dimer is bound in the catalytic valley. Third, the two resulting dsRBD·dsRNA complexes are perpendicular to the α3 helices and the catalytic valley (Figure 3). The E110K mutation appears responsible for the fact that the dsRNA is not bound within the catalytic valley and thus cannot be processed. Therefore, the E110K mutation acts as a catalytic antideterminant of RNase III, uncoupling the dsRNA binding and processing abilities of the enzyme.

The dsRBD Plays the Most Important Role in the Binding of dsRNA
The interaction between the polypeptides and one dsRNA pseudoduplex involves residues on one of the dsRBD and both endoNDs of a dimeric molecule (Figure 3). Upon dsRNA binding, the buried surface between the substrate and protein is approximately 1600, 200, and 400 Å² for the dsRBD, the endoND of the same peptide chain, and the endoND from the other chain, respectively. Accordingly, the three polypeptides contribute to the formation of 25, 3, and 4 direct hydrogen bonds with the dsRNA, respectively. Among the 25 direct hydrogen bonds between the dsRBD and dsRNA, 5 involve guanine base functional groups. The seven

hydrogen bonds between dsRNA and the two endoNDs involve three types of nucleotide atoms (O2′, O3′, and O2P) and 6 amino acid side chains (N61, R63, K32, K96, R97, and K99). In addition, six water molecules mediate additional hydrogen bonds between the dsRBD and dsRNA.

The dsRNA helices in both Aa-E110K·dsRNA (this work) and Xl-dsRBD·dsRNA (Ryter and Schultz, 1998) are formed by the same RNA 10-mer GGCGCGCGCC, permitting a direct comparison of dsRBD-dsRNA interactions in the two complexes. First of all, a difference exists in the relative positioning of the dsRNA with respect to the dsRBD, which can be seen when the two structures are aligned using dsRBD Cα positions. It appears that the dsRNA rotates differentially along its long axis by almost 1 bp while maintaining its interactions with the dsRBD (Figure 4A). Second, Aa-E110K·dsRNA has fewer water-mediated hydrogen bonds between dsRBD and dsRNA than Xl-dsRBD·dsRNA (Ryter and Schultz, 1998). Third, in Aa-E110K·dsRNA, there are 25 direct hydrogen bonds between dsRNA and dsRBD and 5 of these involve nucleotide base functional groups; whereas in Xl-dsRBD·dsRNA, there are only 10 direct hydrogen bonds and 2 involve nucleotide base atoms (Figure 4B). Looking at these interactions more closely, we find that three Aa-dsRBD residues, Q157, Q161, and H179, form the five direct hydrogen bonds with guanine base groups. Q157 in Aa-dsRBD corresponds to Q118 in Xl-dsRBD. However, Q157$_{Aa-dsRBD}$ binds a Gua while Q118$_{Xl-dsRBD}$ recognizes a Cyt (Figure 4B). H179 in Aa-dsRBD corresponds to P140 in Xl-dsRBD, and similarly, H179$_{Aa-dsRBD}$ and P140$_{Xl-dsRBD}$ use their carbonyl oxygen atom for a direct hydrogen bond formation with atom

A

B
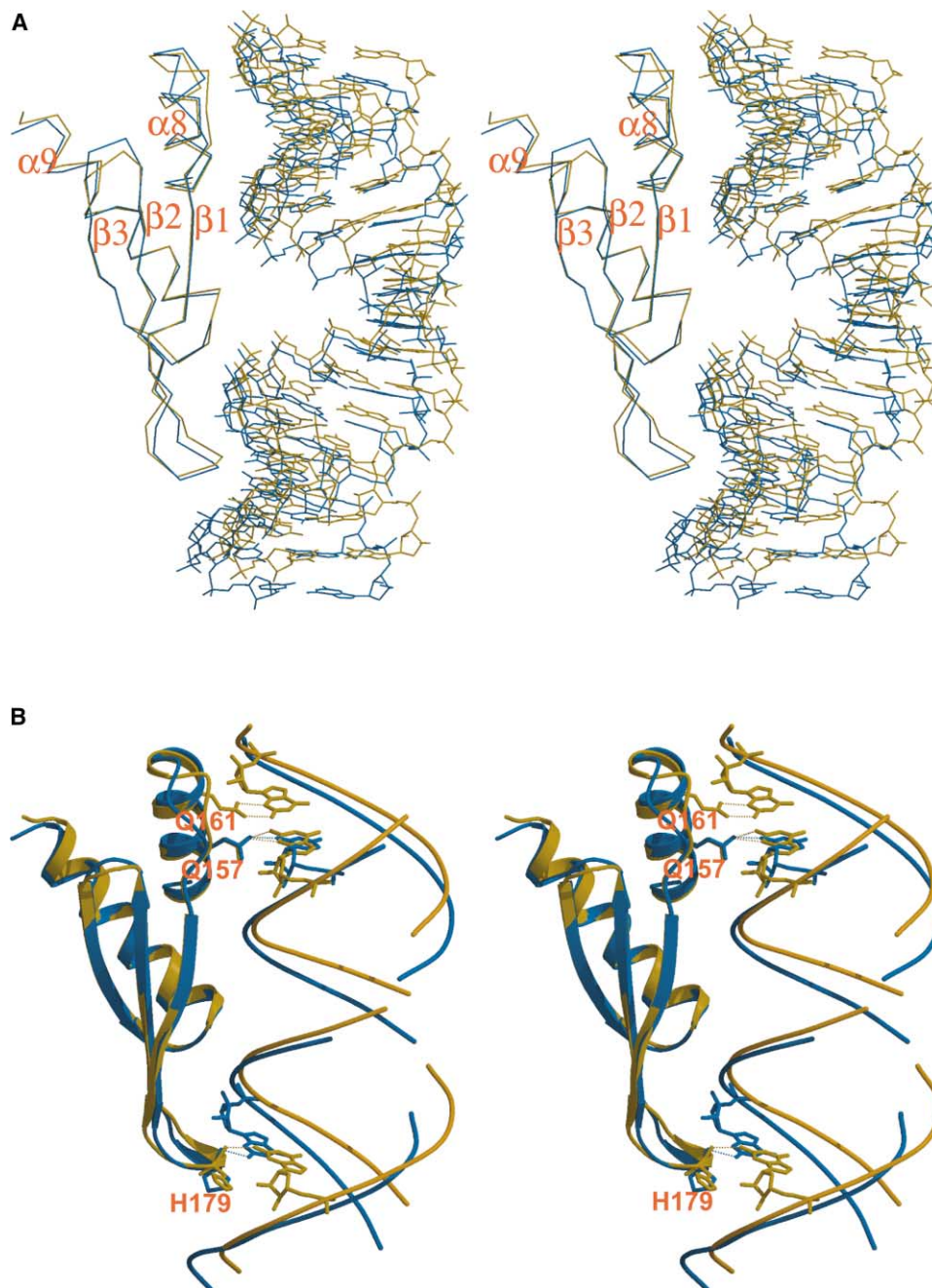
Figure 4. The dsRBD-dsRNA Interaction

(A) Stereoview showing the superposition of the Aa-dsRBD·dsRNA portion (in orange) of Aa-E110K·dsRNA (this work) with Xl-dsRBD·dsRNA (in cyan [Ryter and Schultz, 1998]) on the basis of dsRBD Cα alignment.

(B) Stereoview illustrating the recognition of nucleotide base functional groups by dsRBD residues. Aa-E110K residues Q157, Q161, and H179 (in orange) correspond to Xl-dsRBD residues Q118, V122, and P140 (in cyan), respectively.

N2 of a guanine base. Nevertheless, the guanines recognized by $H179_{Aa-dsRBD}$ and $P140_{Xl-dsRBD}$ are from opposite RNA strands (Figure 4B). Q161 of Aa-dsRBD binds functional groups N2 and N3 of another guanine (Figure 4B), which is unique for Aa-dsRBD because Q161 corresponds to a valine residue in Xl-dsRBD.

Interactions between the dsRBD and dsRNA are pre-

sumably nucleotide sequence independent (Krovat and Jantsch, 1996; Manche et al., 1992; Polson and Bass, 1994; Ryter and Schultz, 1998). On the basis of the crystal structures of Aa-E110K·dsRNA (this work) and Xl-dsRBD·dsRNA (Ryter and Schultz, 1998), it appears that $Q157_{Aa-dsRBD}$ recognizes either a Gua or a Cyt, and $H179_{Aa-dsRBD}$ recognizes a Gua. If any RNA sequence
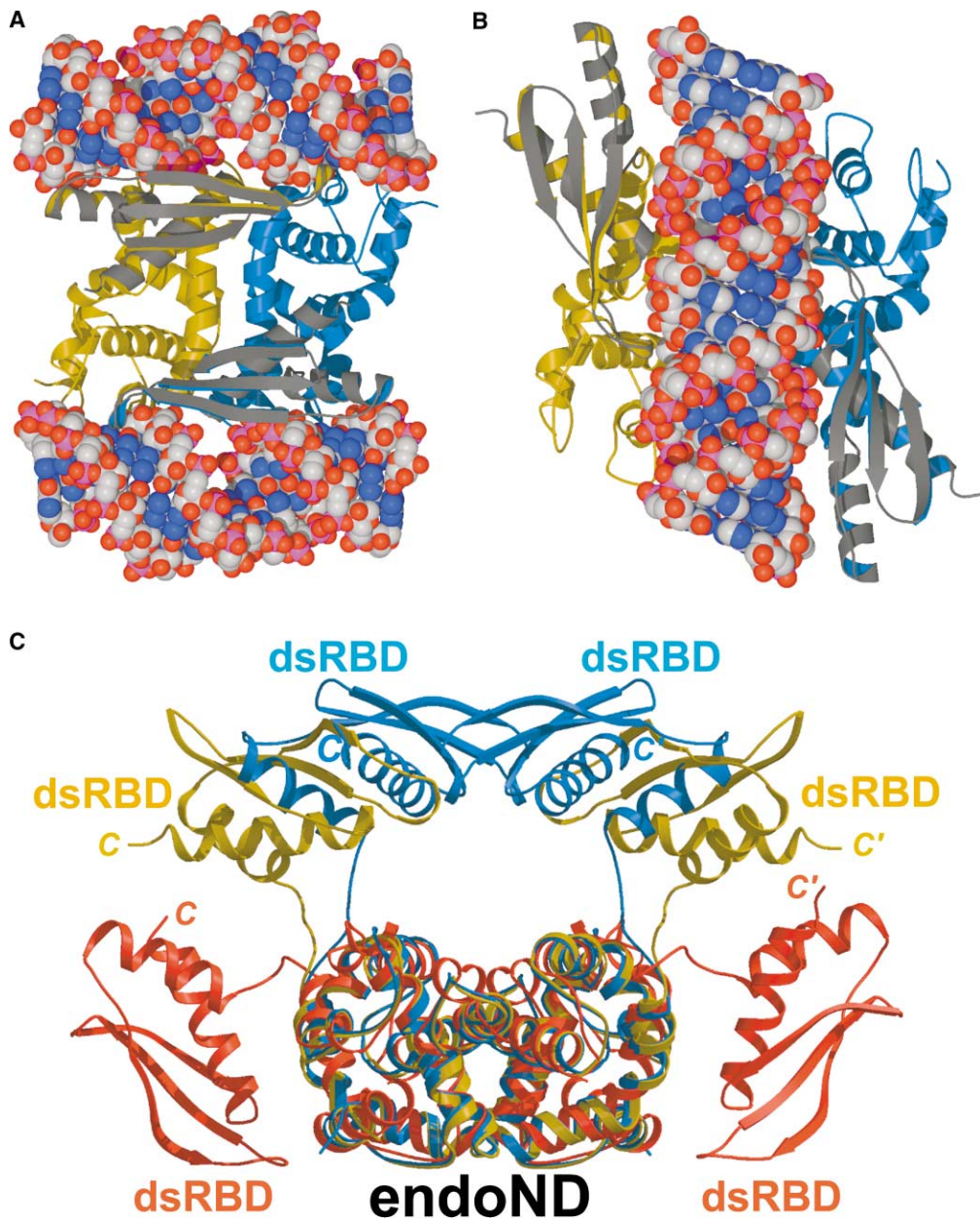
Figure 5. Comparison of Full-Length RNase III Model and Structures

(A) The crystal structure of Aa-E110K·dsRNA (this work).

(B) The model of Aa-RNase III·dsRNA (Blaszczyk et al., 2001). The dsRNA is illustrated as vdw space-filling models in atomic color scheme (carbon in light gray, nitrogen in blue, and oxygen in red). One Aa-E110K chain of the dimer is colored in orange and the other in cyan, and the dsRBD is highlighted with dark gray surfaces.

(C) The alignment, using endoND Cα positions, of the crystal structure of Aa-E110K·dsRNA (in cyan; this work), the model of Aa-RNase III·dsRNA (in orange [Blaszczyk et al., 2001]) and the crystal structure of ligand-free Tm-RNase III (in red, PDB entry 1O0W). The dsRNA is not shown for clarity. The molecular orientation is related to those in (A) and (B) by a 90° rotation around the horizontal axis for an optimal view of the flexible linker between the endoND and dsRBD.

specificity exists for the dsRBD of RNase III, it could only be provided by the highly conserved residue Q161$_{\text{Aa-dsRBD}}$.

Structural Basis of the Genetically Important Linker between the EndoND and dsRBD

Our model of Aa-RNase III·dsRNA (Blaszczyk et al., 2001) suggests the dsRNA-bound form of RNase III as a dsRNA-processing complex, whereas our crystal structure of Aa-E110K·dsRNA (this work) may represent the dsRNA-bound form of RNase III as a noncatalytic assembly. Three major differences exist between the two forms. First, although the conformations of individual domains are nearly identical, the relative orientations of the endoND and dsRBD are dramatically different

(Figures 5A and 5B). Second, in the model of AaRNase III·dsRNA (Blaszczyk et al., 2001), the dsRNA substrate is bound in the catalytic valley; whereas, in the crystal structure of Aa-E110K·dsRNA, neither of the two dsRNA helices is (Figures 5A and 5B). Third, in the model of AaRNase III·dsRNA (Blaszczyk et al., 2001), two dsRBD are parallel to the valley and interact with the same dsRNA helix (Figure 5B). In the crystal structure of Aa-E110K·dsRNA, however, each dsRBD binds a different dsRNA helix and the resulting dsRBD·dsRNA complexes are perpendicular to the valley (Figure 5A). This ∼90° difference in the orientation of dsRNA is readily explained if the linker between the endoND and dsRBD is flexible, which is suggested by available structural information. Figure 5C depicts the superposition of Aa-E110K·dsRNA (this work), Aa-RNase III·dsRNA (Blaszczyk et al., 2001), and Tm-RNase III (PDB entry 1O0W), demonstrating that the flexible linker between the endoND and dsRBD ($_{145}$EGRVKKD$_{151}$ and $_{162}$KGEMLFD$_{168}$ in Aa- and Tm-RNase III, respectively, Figure 1B) allows the dsRBD to rotate and shift dramatically with respect to the endoND. We believe that this flexible linker enables RNase III to assume at least two distinct dsRNA binding modes represented by our model of Aa-RNase III·dsRNA on the one hand and by the crystal structure of Aa-E110K·dsRNA on the other. These two modes of dsRNA binding affect posttranscriptional gene expression by distinct mechanisms. As a dsRNA-processing enzyme, RNase III binds dsRNA in the valley where the active centers are located, allowing the substrate to be processed. As a dsRNA binding protein, RNase III binds dsRNA without processing and influences gene expression by site-specific dsRNA binding (Calin-Jageman and Nicholson, 2003; Court, 1993; Dasgupta et al., 1998). In this binding mode as seen in the crystal structure of Aa-E110K·dsRNA, the protein-bound dsRNA is far away from the enzymatic active centers and thus cannot be processed.

Among the ten missense mutations that cause defects in Ec-RNase III, *rnc10* (Q153P) and *rnc7* (D155E) (Inada and Nakamura, 1995) are located in the linker region (Figure 1). It is readily explainable if the dsRNA-bound form as seen in the Aa-E110K·dsRNA complex is also an intermediate toward the processing form as seen in our model (Blaszczyk et al., 2001). We speculate that the wild-type RNase III dimer in the cell first binds a dsRNA through one of its two dsRBDs. If the dsRNA has sufficient length (at least two helical turns) and does not contain antideterminants (see below for details), an isomerization to the processing form of the enzyme may occur. This isomerization step is dependent upon the flexible linker between the endoND and the dsRBD as well as increased binding affinity to the dsRNA helix afforded by its interaction with the other dsRBD and the catalytic valley of the endoND.

Catalytic Antideterminants of RNase III

The positive expression of CIII and Int in bacteriophage λ are two examples whose genetic control may be exerted by site-specific dsRNA binding of RNase III in the absence of processing (Guarneros, 1988; Oppenheim et al., 1993). In these two special cases, the endoND may still be functional but the respective CIII and Int mRNA may not be bound in the valley that contains the active centers. A special structural motif in the RNA of these two genes might act as an antideterminant for dsRNA processing. The structure of this RNA motif remains to be seen. Very recently, the first direct evidence of RNA structure-dependent uncoupling of substrate recognition and cleavage by the wild-type Ec-RNase III was reported; the R1.1[CL3B], a dsRNA mutant derived from the T7 phage R1.1 RNase III substrate, was selected to be resistant to cleavage in vitro but to retain binding affinity. This mutant RNA contains a special bulge-helix-bulge motif that may act as an antideterminant for catalytic processing (Calin-Jageman and Nicholson, 2003). In light of the structure of Aa-E110K·dsRNA, the bulge-helix-bulge motif in the R1.1[CL3B] may act by blocking the binding of dsRNA in the valley that contains active centers. Therefore, the catalytic antideterminants embedded in the dsRNA may be anti endoND but not anti dsRBD, which may also be the case in ethidium-dependent uncoupling of substrate binding and cleavage by Ec-RNase III (Calin-Jageman et al., 2001) in which two ethidium binding sites exist in the R1.1 RNA and the site-specific binding of ethidium to the RNA substrate perturbs substrate recognition by the endoND.

The catalytic antideterminant of RNase III uncouples the dsRNA binding and processing activities. It can be either a special structural motif embedded in dsRNA (Calin-Jageman et al., 2001; Calin-Jageman and Nicholson, 2003) or a defective mutation in the endoND (this work). In both cases, it is the interaction between the endoND catalytic valley and the dsRNA that is disrupted.

Experimental Procedures

Protein Expression and Purification

The Aa-endoND was overproduced in *E. coli* and purified as described (Blaszczyk et al., 2001). The open reading frame (ORF) encoding full-length Aa-RNase III (GenBank accession: AAC07049) was amplified from genomic DNA by the polymerase chain reaction (PCR) using the following oligonucleotide primers: 5′-GGG GAC AAG TTT GTA CAA AAA AGC AGG CTT TAA GAA GGA GAT ATA CAT ATG AAA ATG TTG GAG CAA CTT G-3′ and 5′-GGG GAC CAC TTT GTA CAA GAA AGC TGG GTT ATT ATT CTG ATT CCT CCA GTA ATT T-3′. The PCR amplicon was inserted into pDONR201 (Invitrogen) by recombinational cloning. Next, E110 was changed to Lys by site-directed mutagenesis and the entire sequence confirmed experimentally. Finally, the Aa-E110K RNase III ORF was recombined into pDEST-42 (Invitrogen) to generate the plasmid expression vector pHPK1409, which produces untagged Aa-E110K RNase III under the control of the bacteriophage T7 promoter. The Aa-E110K RNase III was produced in BL21(DE3)-RIL cells (Stratagene) at 30°C for 18 hr in LB broth supplemented with 100 μg/ml ampicillin, 35 μg/ml chloramphenicol, and 0.2% glucose. Cells were pelleted by centrifugation and stored at −80°C.

Unless otherwise stated, all procedures were performed at 4°C. *E. coli* cell paste was suspended in ice-cold 50 mM sodium phosphate (pH 8.0), 25 mM NaCl buffer (buffer A) containing 1 mM benzamidine and Complete EDTA-free protease inhibitor cocktail tablets (Roche), and disrupted with an APV Gaulin Model G1000 homogenizer at 10,000 psi. The homogenate was centrifuged at 20,000 × g for 30 min, and the supernatant was heat treated at 80°C for 30 min. After pelleting the insoluble material by centrifugation, the supernatant was filtered through a 0.22 μm polyethersulfone membrane and applied to a HiPrep 16/10 SP FF column (Amersham Biosciences) equilibrated with buffer A. The column was washed with 10 column volumes of buffer A and eluted with a linear gradient of NaCl from 25 mM to 1 M. Fractions containing recombinant pro-

Table 1. Data Collection, Structure Determination, and Refinement Statistics

	Aa-endoND·Mg^{2+}	Aa-E110K·dsRNA
Crystal		
Shape	Block	Needle
Dimensions (mm)	0.15, 0.15, 0.20	0.03, 0.05, 0.25
X-Ray Data		
Radiation source	X9B, NSLS	22-ID, APS
Detector type	ADSC Quantum-4 CCD	Bruker Proteum-300 CCD
Wavelength (Å)	1.045	1.000
Space group	P2$_1$	C222$_1$
Unit-cell parameters		
a (Å)	49.74	58.29
b (Å)	140.86	118.14
c (Å)	49.75	106.67
β (°)	117.29	90.0
Resolution (Å)	30.0–2.30	50.0–2.15
Measured reflections	68,942	95,376
Unique reflections	24,431	18,881
Completeness (%), overall/last shell[a]	89.4/87.4	92.3/58.3
R$_{merge}$[b], overall/last shell	0.076/0.279	0.058/0.262
I/σ(I), overall/last shell	13.9/3.7	22.0/1.8
Molecular Replacement		
Search model	PDB entry 1I4S	PDB entry 1I4S
Correlation coefficient	0.61	0.43
R factor	0.39	0.47
Refinement and Statistics		
Reflections in refinement	22,942	17,624
Reflections for R$_{free}$ calculation	1,248	1,091
No. residues/protein atoms	594/4,929	220/1,838
No. heterogen atoms	4 (Mg^{2+})	848 (RNA), 8 (Tris)
No. water oxygen atoms	675	236
Final R$_{free}$	0.255	0.242
Final R factor	0.215	0.192
Rms deviation (Å)		
Bond lengths	0.004	0.005
Bond angles	0.016	0.026
Estimated coordinate error (Å)	0.25	0.26
Overall B$_{iso}$ (Å^2)	34.6	47.2
Wilson B factor (Å)	32.8	44.7
Ramachandran statistics (%):		
Most favored φ/ψ values	91.8	96.1
Disallowed φ/ψ values	0.0	0.0

[a] 2.38–2.30 and 2.23–2.15 Å for Aa-endoND·Mg^{2+} and Aa-E110K·dsRNA, respectively.
[b] R$_{merge}$ = Σ|(I − <I>)|/Σ(I), where I is the observed intensity.

tein were pooled, concentrated using an YM10 membrane (Amicon), and fractionated on a HiLoad 26/60 Superdex 75 pg column (Amersham Biosciences) equilibrated in 25 mM Tris (pH 7.2), 600 mM NaCl buffer. Fractions containing Aa-E110K were pooled and diluted with a 50 mM Tris (pH 7.5) buffer to reduce the NaCl concentration to 300 mM. The sample was applied to a 15 ml AGPoly(I)·Poly(C) Type 6 column (Amersham Biosciences) equilibrated with 50 mM Tris (pH 7.5), 300 mM NaCl buffer. The column was washed extensively with equilibration buffer until a stable baseline was reached, then eluted with a linear gradient of NaCl from 0.3 to 1 M. Fractions containing recombinant protein were pooled, concentrated, and subjected to a second round of size exclusion chromatography as described above. The final product was diluted with a 25 mM Tris (pH 7.2) buffer to reduce the NaCl concentration to 300 mM and concentrated to 17.4 mg/ml (determined spectrophotometrically using a molar extinction coefficient of 24,180 M^{-1}cm^{-1}). Aliquots were flash-frozen in liquid nitrogen and stored at −80°C until use. The Aa-E110K protein was judged to be >95% pure by sodium dodecyl sulfate-polyacrylamide gel electrophoresis. The molecular weight was confirmed by electrospray mass spectrometry.

RNA 10-mer GGCGCGCGCC

The self-complementary RNA 10-mer (GGCGCGCGCC) (Ryter and Schultz, 1998) was purchased from the Keystone Labs (Camarillo, CA) and dissolved at 0.75 mM concentration in 25 mM Tris-HCl (pH 7.2) buffer containing 0.2 M NaCl.

Crystallization and X-Ray Diffraction Data Acquisition

Crystals were grown using the hanging-drop vapor diffusion method at 19°C ± 1°C. The drops contained equal volumes of protein and reservoir solutions. For Aa-endoND·Mg^{2+}, the protein concentration was 13 mg/ml in 25 mM Tris-HCl (pH 7.5) buffer containing 600 mM NaCl and 1.5 mM MgCl$_2$, and the reservoir solution was composed of 30% (w/v) PEG 4000 and 0.2 M sodium acetate in 100 mM Tris-HCl (pH 8.5) buffer. For Aa-E110K·dsRNA, the protein concentration was 10 mg/ml and the RNA concentration was 0.075 mM in 25 mM Tris-HCl (pH 7.2) containing 200 mM NaCl and 1.5 mM MgCl$_2$, and the reservoir solution was composed of 24% (w/v) PEG 4000, 0.4 M imidazolel, and 0.16 M ammonium acetate in 100 mM Tris-HCl (pH 8.5) buffer. Data processing was carried out with the HKL2000 program suite (Otwinowski and Minor, 1997). Crystal data and pro-

cessing statistics are summarized in Table 1. Further data processing was carried out with the CCP4 suite (CCP4, 1994) for structure determination and refinement.

Structure Determination and Refinement
The structures of Aa-endoND·Mg^{2+} and Aa-E110K·dsRNA were determined with the molecular replacement program AMoRe (Navaza, 1994) using X-ray diffraction data within the resolution range of 10–4 Å. For the Aa-endoND·Mg^{2+} structure, the dimer of ligand-free Aa-endoND structure (Blaszczyk et al., 2001) was the search model. For the Aa-E110K·dsRNA structure, a monomer of ligand-free Aa-endoND structure (Blaszczyk et al., 2001) was the search model. Solvent molecules were excluded from the search models. The partial structure of Aa-E110K·dsRNA, containing the endoND only, was subject to rigid body refinement, energy minimization, and grouped B factor refinement followed by difference Fourier synthesis, which revealed the position of dsRBD and dsRNA. Accordingly, a complete model of Aa-E110K·dsRNA was built, consisting of an Aa-E110K chain and two 10 bp dsRNA helices. The crystal structure of Aa-endoND·Mg^{2+} was initially refined with the simulated annealing procedure (Brünger and Rice, 1997) of CNS (Brünger et al., 1998) followed by least-squares refinement with SHELXL (Sheldrick and Schneider, 1997). The refinement of Aa-E110K·dsRNA was carried out with CNS (Brünger et al., 1998) only. Bulk solvent correction was employed during the refinement. All graphics work was carried out using O (Jones et al., 1991). The refined structures were assessed using PROCHECK (Laskowski et al., 1993). Illustrations were generated with program packages MOLSCRIPT (Kraulis, 1991), BOBSCRIPT (Esnouf, 1997), and RASTER3D (Merritt and Bacon, 1997).

References

Bardwell, J.C., Regnier, P., Chen, S.M., Nakamura, Y., Grunberg-Manago, M., and Court, D.L. (1989). Autoregulation of RNase III operon by mRNA processing. EMBO J. *8*, 3401–3407.

Bernstein, E., Caudy, A.A., Hammond, S.M., and Hannon, G.J. (2001). Role for a bidentate ribonuclease in the initiation step of RNA interference. Nature *409*, 363–366.

Blaszczyk, J., Tropea, J.E., Bubunenko, M., Routzahn, K.M., Waugh, D.S., Court, D.L., and Ji, X. (2001). Crystallographic and modeling studies of RNase III suggest a mechanism for double-stranded RNA cleavage. Structure *9*, 1225–1236.

Brünger, A.T., and Rice, L.M. (1997). Crystallographic refinement by simulated annealing: methods and applications. Methods Enzymol. *277*, 243–269.

Brünger, A.T., Adams, P.D., Clore, G.M., DeLano, W.L., Gros, P., Grosse-Kunstleve, R.W., Jiang, J.S., Kuszewski, J., Nilges, M., Pannu, N.S., et al. (1998). Crystallography & NMR system: a new software suite for macromolecular structure determination. Acta Crystallogr. D *54*, 905–921.

Bycroft, M., Grunert, S., Murzin, A.G., Proctor, M., and St Johnston, D. (1995). NMR solution structure of a dsRNA binding domain from *Drosophila staufen* protein reveals homology to the N-terminal domain of ribosomal protein S5. EMBO J. *14*, 3563–3571.

Calin-Jageman, I., and Nicholson, A.W. (2003). RNA structure-dependent uncoupling of substrate recognition and cleavage by *Escherichia coli* ribonuclease III. Nucleic Acids Res. *31*, 2381–2392.

Calin-Jageman, I., Amarasinghe, A.K., and Nicholson, A.W. (2001). Ethidium-dependent uncoupling of substrate binding and cleavage by Escherichia coli ribonuclease III. Nucleic Acids Res. *29*, 1915–1925.

Carthew, R.W. (2001). Gene silencing by double-stranded RNA. Curr. Opin. Cell Biol. *13*, 244–248.

CCP4 (Collaborative Computational Project 4) (1994). The CCP4 suite: programs for protein crystallography. Acta Crystallogr. D *50*, 760–763.

Court, D. (1993). RNA processing and degradation by RNase III. In Control of Messenger RNA Stability, J.G. Belasco and G. Braverman, eds. (New York: Academic Press), pp. 71–116.

Dasgupta, S., Fernandez, L., Kameyama, L., Inada, T., Nakamura, Y., Pappas, A., and Court, D.L. (1998). Genetic uncoupling of the dsRNA-binding and RNA cleavage activities of the *Escherichia coli* endoribonuclease RNase III - the effect of dsRNA binding on gene expression. Mol. Microbiol. *28*, 629–640.

Davidov, Y., Rahat, A., Flechner, I., and Pines, O. (1993). Characterization of the *rnc-97* mutation of RNase III: a glycine to glutamate substitution increases the requirement for magnesium ions. J. Gen. Microbiol. *139*, 717–724.

Dunn, J.J. (1982). Ribonuclease III. In The Enzymes, P. Boyer, ed. (New York: Academic Press), pp. 485–499.

Esnouf, R.M. (1997). An extensively modified version of MolScript that includes greatly enhanced coloring capabilities. J. Mol. Graph. Model. *15*, 112–113, 132–134.

Filippov, V., Solovyev, V., Filippova, M., and Gill, S.S. (2000). A novel type of RNase III family proteins in eukaryotes. Gene *245*, 213–221.

Guarneros, G. (1988). Retroregulation of bacteriophage lambda int gene expression. Curr. Top. Microbiol. Immunol. *136*, 1–19.

Inada, T., and Nakamura, Y. (1995). Lethal double-stranded RNA processing activity of ribonuclease III in the absence of suhB protein of *Escherichia coli*. Biochimie *77*, 294–302.

Inada, T., Kawakami, K., Chen, S.M., Takiff, H.E., Court, D.L., and Nakamura, Y. (1989). Temperature-sensitive lethal mutant of ERA, a G protein in *Escherichia coli*. J. Bacteriol. *171*, 5017–5024.

Jones, T.A., Zou, J.Y., Cowan, S.W., and Kjeldgaard, M. (1991). Improved methods for building protein models in electron density maps and the location of errors in these models. Acta Crystallogr. A *47*, 110–119.

Kharrat, A., Macias, M.J., Gibson, T.J., Nilges, M., and Pastore, A. (1995). Structure of the dsRNA binding domain of E. coli RNase III. EMBO J. *14*, 3572–3584.

Krainer, A. (1997). Eukaryotic mRNA Processing (New York: IRL Press).

Kraulis, P.J. (1991). MOLSCRIPT: a program to produce both detailed and schematic plots of protein structures. J. Appl. Crystallogr. *24*, 946–950.

Krovat, B.C., and Jantsch, M.F. (1996). Comparative mutational analysis of the double-stranded RNA binding domains of Xenopus laevis RNA-binding protein A. J. Biol. Chem. *271*, 28112–28119.

Lamontagne, B., Larose, S., Boulanger, J., and Elela, S.A. (2001). The RNase III family: a conserved structure and expanding functions in eukaryotic dsRNA metabolism. Curr. Issues Mol. Biol. *3*, 71–78.

Laskowski, R.A., MacArthur, M.W., Moss, D.S., and Thornton, J.M. (1993). PROCHECK: a program to check stereochemical quality of protein structures. J. Appl. Crystallogr. *26*, 283–291.

Li, H., and Nicholson, A.W. (1996). Defining the enzyme binding domain of a ribonuclease III processing signal. Ethylation interference and hydroxyl radical footprinting using catalytically inactive RNase III mutants. EMBO J. *15*, 1421–1433.

Manche, L., Green, S.R., Schmedt, C., and Mathews, M.B. (1992). Interactions between double-stranded RNA regulators and the protein kinase DAI. Mol. Cell. Biol. *12*, 5238–5248.

Merritt, E.A., and Bacon, D.J. (1997). Raster3D: photorealistic molecular graphics. Methods Enzymol. *277*, 505–524.

Nanduri, S., Carpick, B.W., Yang, Y., Williams, B.R., and Qin, J. (1998). Structure of the double-stranded RNA-binding domain of

the protein kinase PKR reveals the molecular basis of its dsRNA-mediated activation. EMBO J. *17*, 5458–5465.

Nashimoto, H., and Uchida, H. (1985). DNA sequencing of the *Escherichia coli* ribonuclease III gene and its mutations. Mol. Gen. Genet. *201*, 25–29.

Navaza, J. (1994). An automated package for molecular replacement. Acta Crystallogr. A *50*, 157–163.

Nicholson, A.W. (1996). Structure, reactivity, and biology of double-stranded RNA. Prog. Nucleic Acid Res. Mol. Biol. *52*, 1–65.

Nicholson, A.W. (1999). Function, mechanism and regulation of bacterial ribonucleases. FEMS Microbiol. Rev. *23*, 371–390.

Oppenheim, A.B., Kornitzer, D., Altuvia, S., and Court, D.L. (1993). Posttranscriptional control of the lysogenic pathway in bacteriophage lambda. Prog. Nucleic Acid Res. Mol. Biol. *46*, 37–49.

Otwinowski, Z., and Minor, W. (1997). Processing of X-ray diffraction data collected in oscillation mode. Methods Enzymol. *276*, 307–326.

Polson, A.G., and Bass, B.L. (1994). Preferential selection of adenosines for modification by double-stranded RNA adenosine deaminase. EMBO J. *13*, 5701–5711.

Ramos, A., Grunert, S., Adams, J., Micklem, D.R., Proctor, M.R., Freund, S., Bycroft, M., St Johnston, D., and Varani, G. (2000). RNA recognition by a Staufen double-stranded RNA-binding domain. EMBO J. *19*, 997–1009.

Robertson, H.D. (1982). *Escherichia coli* ribonuclease III cleavage sites. Cell *30*, 669–672.

Robertson, H.D., and Dunn, J.J. (1975). Ribonucleic acid processing activity of *Escherichia coli* ribonuclease III. J. Biol. Chem. *250*, 3050–3056.

Robertson, H.D., Webster, R.E., and Zinder, N.D. (1968). Purification and properties of ribonuclease III from *Escherichia coli*. J. Biol. Chem. *243*, 82–91.

Ryter, J.M., and Schultz, S.C. (1998). Molecular basis of double-stranded RNA-protein interactions: structure of a dsRNA-binding domain complexed with dsRNA. EMBO J. *17*, 7505–7513.

Sheldrick, G.M., and Schneider, T.R. (1997). SHELXL: high-resolution refinement. Methods Enzymol. *277*, 319–343.

Sun, W., and Nicholson, A.W. (2001). Mechanism of action of *Escherichia coli* ribonuclease III. Stringent chemical requirement for the glutamic acid 117 side chain and Mn(2+) rescue of the Glu117Asp mutant. Biochemistry *40*, 5102–5110.

Wu, H., Xu, H., Miraglia, L.J., and Crooke, S.T. (2000). Human RNase III is a 160-kDa protein involved in preribosomal RNA processing. J. Biol. Chem. *275*, 36957–36965.

Zamore, P.D. (2001). Thirty-three years later, a glimpse at the ribonuclease III active site. Mol. Cell *8*, 1158–1160.

Accession Numbers

The coordinates and structure factors (entries 1RC5 and 1RC7 for Aa-endoND·Mg^{2+} and Aa-E110K·dsRNA, respectively) have been deposited in the Protein Data Bank (Rutgers, The State University of New Jersey).